Surface formation routes of interstellar molecules : a laboratory study

Sergio, I.

CHAPTER 5

Water formation at low temperatures by surface O_2 hydrogenation II: the reaction network[1]

Water is abundantly present in the Universe. It is the main component of interstellar ice mantles and a key ingredient for life. Water in space is mainly formed through surface reactions. Three formation routes have been proposed in the past: hydrogenation of surface O, O_2, and O_3. In Chapter 3 we discussed an unexpected non-standard zeroth order H_2O_2 production behavior in O_2 hydrogenation experiments, which suggests that the proposed reaction network is not complete, and that the reaction channels are probably more interconnected than previously thought. In this chapter we aim to derive the full reaction scheme for O_2 surface hydrogenation and to constrain the rates of the individual reactions. This is achieved through simultaneous H-atom and O_2 deposition under ultra-high vacuum conditions for astronomically relevant temperatures. Different H/O_2 ratios are used to trace different stages in the hydrogenation network. The chemical changes in the forming ice are followed by means of Reflection Absorption Infrared Spectroscopy (RAIRS). New reaction paths are revealed as compared to previous experiments. Several reaction steps prove to be much more efficient ($H + O_2$) or less efficient ($H + OH$ and $H_2 + OH$) than originally thought. These are the main conclusions of this work and the extended network concluded here will have profound implications for models that describe the formation of water in space.

[1] Based on: H. M. Cuppen, S. Ioppolo, C. Romanzin, H. Linnartz, 2008, 2010, Physical Chemistry Chemical Physics, volume 12, pages 12077-12088

5.1 Introduction

Water is the simplest stable compound of the two most common reactive elements, O and H, and is abundantly present throughout the Universe. It is the main component of interstellar (Whittet et al. 1988, Boogert et al. 2008) and cometary ices (Bockelée-Morvan et al. 2000) and both types of ices are believed to play an important role in the delivery of water to Earth in the early times of our Solar System. Water is considered an essential ingredient for the formation of life but it is surprising that its own formation mechanism is not fully understood.

Water in the interstellar medium (ISM) is predominantly formed through surface reactions on interstellar dust particles. Three reaction routes have been proposed: hydrogenation of atomic oxygen, molecular oxygen and ozone (Tielens & Hagen 1982). These formation routes in the solid phase have been the topic of several laboratory studies in recent years. The hydrogenation routes through atomic oxygen and ozone have been studied by Hiraoka et al. (1998) and Dulieu et al. (2010); and Mokrane et al. (2009) and Romanzin et al. (2010). Here we focus on the hydrogenation of molecular oxygen via the reaction scheme

$$H + O_2 \rightarrow HO_2, \tag{5.1}$$

$$H + HO_2 \rightarrow H_2O_2, \tag{5.2a}$$

$$H + H_2O_2 \rightarrow H_2O + OH, \tag{5.3}$$

and

$$H + OH \rightarrow H_2O, \tag{5.4}$$

as proposed by Tielens & Hagen (1982). Our and other experimental studies of the hydrogenation of O_2 ice indeed showed the formation of hydrogen peroxide and water (Miyauchi et al. 2008, Ioppolo et al. 2008, Matar et al. 2008), but the results also raised several unanswered questions. As discussed in Chapter 4, the formation of H_2O_2 shows zeroth order kinetics, whereas first order kinetics are expected. We hypothesized that penetration of hydrogen atoms into the oxygen ice causes this effect. Molecular oxygen ice has unique properties, as compared to CO and H_2O ice, and allows hydrogen atoms to penetrate deep into the ice, depending on the ice temperature. In Chapter 4 this mechanism was indeed shown to explain the observed zeroth order behavior. Our second puzzling observation was the fact that we did not observe an isotope effect in reaction (5.3) whereas this is expected due to its relatively large barrier. This point is made later by Oba et al. (2009) as well. Reactions with barriers at low temperatures generally proceed via tunnelling and this would here result in a faster hydrogenation than deuteration rate. This was not observed. In Ioppolo et al. (2008) we promised to address this point in a later paper and here we suggest that reactions (5.1)-(5.4) may not be the only reactions involved in the formation of water when hydrogenating O_2 ice and that the incomplete reaction network of the model artificially resulted in an isotope-independent reaction rate. An additional indication for this is the observation that the water ice formation rate does not seem to increase with the amount of H_2O_2 and this is expected if H_2O_2 is its only precursor.

The present chapter focuses on the reactions involved in the hydrogenation of pure oxygen ice. This is done by co-deposition experiments of O_2 molecules and H atoms. This is intrinsically different from the method used in Chapter 4 where the O_2 ice was prepared first and then sequentially exposed to hydrogen atoms. By changing the stoichiometric ratios of O_2 and H, different stages of the formation route through reactions (5.1)-(5.4) become experimentally accessible. This gives us the unique opportunity to probe also the reactive intermediates. In all previous studies only the stable intermediate H_2O_2- and final H_2O-products were recorded. Oba et al. (2009) performed similar co-deposition experiments using a very high H/O_2 ratio with the aim to study the structure of the obtained water ice. This mainly gave information about the final products but not about the individual reaction routes. Since the conditions in the interstellar medium vary and also differ from the laboratory conditions — especially in terms of atom fluxes — it is very important to obtain detailed information about the surface reaction routes. In a Monte Carlo study of water ice formation in diffuse, translucent and dark clouds, Cuppen & Herbst (2007) showed that the dominant water formation route is determined by the environment (temperature and H/H_2 ratio). However, the reaction scheme used in these simulations was based on gas phase data and not tested for surface reactions. In the present chapter, a range of different O_2/H ratios are applied to probe different hydrogenation stages. Three different astronomically relevant surface temperatures of 15, 20 and 25 K are used to check for thermally activated processes. The highest temperature, 25 K, is chosen to be just below the desorption temperature of molecular oxygen (Acharyya et al. 2007). The overall goal is to derive the full reaction network and to constrain reaction rates for the individual reactions. We will show that indeed a number of extra reaction paths should be considered to complete the initially proposed reaction network and that the O_2 hydrogenation channel is interconnected with the O and O_3 production channels.

5.2 Experimental and data analysis

5.2.1 Experimental

All experiments are performed in an ultra high vacuum setup (SURFRESIDE) with a room temperature base pressure in the 10^{-10} mbar regime. A detailed description of the experiment is given in Chapter 4 and here only a brief explanation is given with the focus on the difference in methodology with respect to the previous study in Chapter 4. Hydrogen atoms and molecules and oxygen molecules are deposited simultaneously on a gold coated copper substrate in the center of the main chamber which is temperature controlled by a close-cycle He cryostat. Temperatures as low as 12 K can be reached with a relative precision of 0.5 K and an absolute temperature accuracy better than 2 K. An all-metal leak valve is used to admit O_2 gas (99.999% purity, Praxair) into the chamber. Deposition of O_2 proceeds under an angle of 45° and with a controllable flow between 10^{-8} and 10^{-7} mbar. A pressure of 10^{-7} mbar corresponds to an O_2 flux of 2.5×10^{13} molecules cm^{-2} s^{-1} (see Chapter 4).

A second precision leak valve is used to admit H_2 molecules (99.8% purity, Praxair) into the capillary of a well-characterized thermal cracking source (Tschersich & von Bonin 1998, Tschersich et al. 2008). For a standard flux, this capillary is heated to 2150 K by a surrounding tungsten filament. A stable H + H_2 flow is obtained in this way. The beam enters the main chamber through a nose-shape quartz pipe, which is designed to collisionally cool the H atoms to room temperature while keeping the number of recombinations of H to H_2 to a minimum and is guided to the surface under 90°. The quartz pipe is designed such that atoms and molecules have a minimum of four collisions before impinging on the ice substrate and are therefore fully collisionally cooled. The final H-atom flux at the surface is measured to be 2.5×10^{13} atoms cm^{-2} s^{-1} under our standard conditions within a factor of two. By changing the filament temperature and/or the H_2 inlet flow, the H-atom flux can be varied between 10^{12}–10^{14} atoms cm^{-2} s^{-1}. Absolute vales are determined as described in Chapter 4. Relative flux accuracies are estimated to be within a factor of 50%. Between the experiments the H/O_2 ratio is varied. This is achieved by varying the O_2 inlet flow and keeping the H-atom flux constant.

Ices are monitored by means of RAIRS using a Fourier Transform infrared spectrometer (FTIR) with a spectral coverage between 4000 and 700 cm^{-1}. A resolution of 0.5 cm^{-1} is used and 128 scans are co-added for one spectrum.

5.2.2 Data analysis

Although O_2 as a diatomic homonuclear molecule is infrared in-active and only gives a small contribution in a water-rich environment (Ehrenfreund et al. 1992), deposition of O_2 has an effect on the baseline of the RAIR spectra. This can be seen in Fig. 5.1a which shows a reference spectrum taken after an O_2 and H_2 co-deposition experiment. The spectrum is completely determined by the deposition of O_2 and the experiments indicate that the distortion of the baseline is directly proportional to the amount of O_2 present in the ice.

For the H and O_2 co-deposition experiments, we assume that the resulting ice at low H/O_2 ratios mainly consists of O_2 and that the baseline distortion is similar to the reference experiment with H_2. Figure 5.1b shows an example spectrum before baseline subtraction for $H/O_2 = 2$ at 20 K. To correct for the influence of O_2, the baseline subtraction consists of two steps for $H/O_2 = 1$ and 2. For $H/O_2 = 10$, we assume that most O_2 is converted to H_2O_2 and indeed here the baseline distortion is minimal. First, a reference spectra (Fig. 5.1a) based on the O_2 and H_2 co-deposition spectrum after a similar fluence of O_2 is subtracted. As a second step, which is applied for all H/O_2 ratios, a piecewise straight baseline is subtracted. A resulting spectrum is shown in Fig. 5.1c for a H/O_2 ratio of 2 and a surface temperature of 20 K. This spectrum (with inset) is also shown in the third panel from the top in Fig. 5.2 and clearly consists of a forest of different features. The bands that we have been able to identify are indicated in Fig. 5.2 and summarized in Table 5.1. All intermediate species from the reaction scheme (5.1)-(5.4) are observed as well as O_3 which is not part of this scheme. A small O_2 feature becomes visible due to interactions with water. Two unidentified features appear at 1420 and 1430 cm^{-1}.

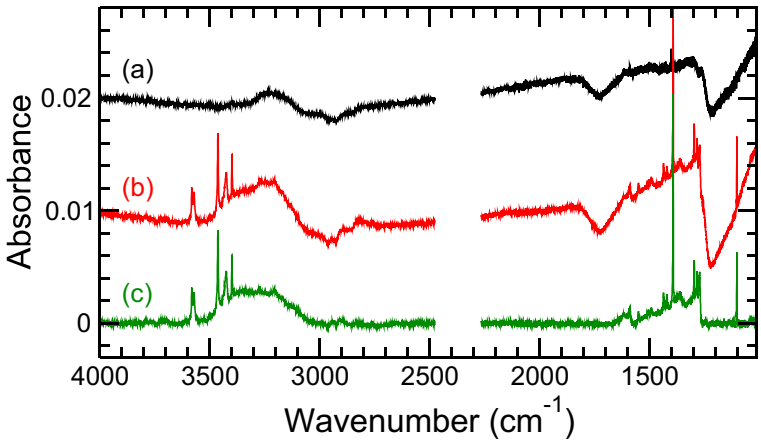

Figure 5.1 RAIR spectra of co-deposited O_2 and H_2 without baseline subtraction (a), co-deposited O_2 and H without baseline subtraction (b), and co-deposited O_2 and H with baseline subtraction (c). H/O_2 or H_2/O_2 is 2 and the surface temperature is 20 K. The spectra (b) and (c) are displaced on the vertical axis by 0.01 and 0.02, respectively.

The formation trends are followed by integrating the corresponding band area as a function time. Because of the overlapping features and because bandstrength information is not available for unstable species like HO_2 and OH, no absolute values are given. The asterisk in Table 5.1 marks the features that have been used for integration and relative quantification. In the case of overlapping bands, Gaussian fits are used to separate the individual contributions.

Table 5.1 Assigned infrared features with their corresponding reference

Position[1] (cm^{-1})	Species	Mode	Reference
1037	O_3	ν_3	Sivaraman et al. (2007)
1100	HO_2	ν_3	Bandow & Akimoto (1985)
1272	H_2O_2	ν_6	Catalano & Sanborn (1963), Lannon et al. (1971)
1282	H_2O_2	ν_6	Catalano & Sanborn (1963), Lannon et al. (1971)
1296	H_2O_2	ν_6	Catalano & Sanborn (1963), Lannon et al. (1971)
1370 (∗)	H_2O_2 (bulk)	ν_2, ν_6, $2\nu_4$	Giguère & Harvey (1959)
1392 (∗)	HO_2	ν_2	Bandow & Akimoto (1985)
1550	O_2	ν_1	Loeffler et al. (2006)
1590 (∗)	H_2O	ν_2	Bandow & Akimoto (1985)
1600 (∗)	H_2O	ν_2	Bandow & Akimoto (1985)
1650 (∗)	H_2O (bulk)	ν_2	Gerakines et al. (1995)
2810	H_2O_2 (bulk)	$2\nu_6$	Giguère & Harvey (1959)
3270	H_2O_2 (bulk)	ν_1, ν_5	Giguère & Harvey (1959)
3240	H_2O (bulk)	ν_1, ν_3	Gerakines et al. (1995)
3400	HO_2	ν_1	Bandow & Akimoto (1985)
3426 (∗)	OH	ν_1(OH-stretch)	Acquista et al. (1968)
3463 (∗)	OH	ν_1(OH-stretch)	Acquista et al. (1968)
3572 (∗)	H_2O_2	ν_5 (OH-stretch)	Catalano & Sanborn (1963), Khriachtchev et al. (2000)
3581 (∗)	H_2O_2	ν_5 (OH-stretch)	Catalano & Sanborn (1963), Khriachtchev et al. (2000)

[1] Asterisks mark the features used to the determine the integrated absorption.

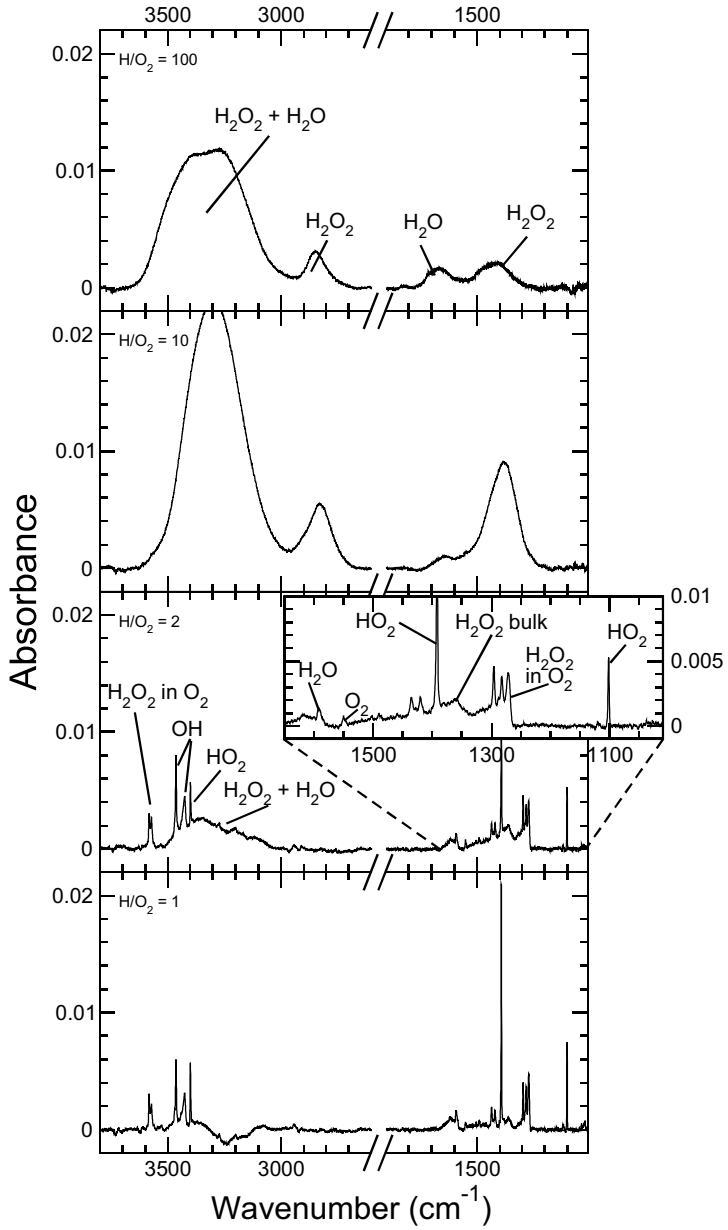

Figure 5.2 RAIR spectra of H and O_2 co-deposition experiments performed for a surface temperature of 20 K and different H/O_2 ratios of 100, 10, 2, and 1 from top to bottom. The H-atom fluence is the same for all spectra.

The spectral appearance of both the H_2O and H_2O_2 bands strongly depends on the environment. In an oxygen-rich environment the bands are narrow. In the remainder of the chapter we will refer to these features as monomer bands, since they are mainly due to single H_2O or H_2O_2 molecules in a hydrophobic environment, in this case the O_2 matrix. By increasing the amount of hydrophilic material in the ice, the bands broaden and the peak positions shift. These we define as bulk bands since they are caused by H_2O or H_2O_2 in an H_2O- or H_2O_2-rich environment. Multiple infrared studies have shown the presence of both bulk and monomer features (Giguère & Harvey 1959, Catalano & Sanborn 1963, Lannon et al. 1971, Bandow & Akimoto 1985, Gerakines et al. 1995, Khriachtchev et al. 2000). For H_2O_2 the bulk and monomer contributions are separated (3572 and 3581 cm^{-1} vs. 1370 cm^{-1}, respectively). The OH-stretch monomer features of H_2O at 3724 and 3732 cm^{-1} are not observed and we therefore conclude that water is not abundantly formed in O_2-rich environments. Only the integrated absorption of the bulk water feature at 1650 cm^{-1} is given for O_2-poor environments. In general the water estimation has the largest error, since the 1550−1700 cm^{-1} range is affected by O_2 baseline distortion and the broad bulk H_2O_2 feature.

5.3 Results

5.3.1 H/O_2 ratio dependence

The ratio between the deposition of H atoms and O_2 molecules determines the hydrogenation grade. Four H atoms are required to fully hydrogenate O_2 to two H_2O molecules. The top panel of Fig. 5.2 shows the RAIR spectrum of the highest H/O_2 ratio that we can reliably reach, which is $H/O_2 = 100$. This spectrum is clearly dominated by broad H_2O and H_2O_2 bands. In this experiment roughly equal amounts of H_2O and H_2O_2 are produced. Oba et al. (2009) produced even more H_2O dominated ices in this way using a higher H/O_2 ratio of 500.

In the present chapter, we are particularly interested in the oxygen dominated regime, where full hydrogenation cannot be reached. Because of the constant supply of O_2, intermediate species are locked in the ice mantle. In this way, all intermediate species listed in Table 5.1 — HO_2, H_2O_2, and OH — can be observed. The first intermediate, HO_2, is clearly present in a very oxygen-rich environment. This is reflected by monomer bands at 1100, 1392, and 3400 cm^{-1} in the spectrum of the bottom panel of Fig. 5.2 for an H/O_2 ratio of 1. In the same spectrum, also H_2O_2 and OH features appear (both monomer features). The presence of the OH features is rather surprising since OH is only formed in reaction (5.3) of the proposed reaction scheme and this reaction is expected to be reached at a higher level of hydrogenation. Furthermore, H_2O, which is formed in the same reaction, is not abundantly present in this spectrum. The third panel of Fig. 5.2 shows a spectrum obtained after exposure of the same H-atom fluence but with an O_2 flow that is reduced by a factor of 2. Here, the HO_2 features shrink, whereas the H_2O_2 and OH signals appear to increase slightly. The H_2O features are small and do not grow and are mostly likely due to background water in the chamber since control experiments of H_2

and O_2 co-deposition result in similar amounts of H_2O. If the oxygen flow is further reduced (second panel, Fig. 5.2), broad bulk water bands can be clearly identified, which are consistent with H_2O formation and in addition the H_2O_2 bands broaden and shift. The spectral features of the intermediates OH and HO_2 disappear entirely.

5.3.2 O_3 detection

For specific conditions, O_3 can be detected as well. Figure 5.3 zooms in on the 1038 cm^{-1} ozone band for three different temperatures and three different H/O_2 ratios. This O_3 band is rather broad and appears to consist of several contributions. As discussed in Sivaraman et al. (2007) it is very sensitive to the local environment and can shift over more than ten wavenumbers. Ozone appears to be predominantly present in the low temperature spectra (15 and 20 K) and for low H/O_2 ratios, or at the opposite conditions: high temperature (25 K) and high H/O_2 ratio. Its presence indicates that oxygen atoms are involved at some stage in the reaction scheme, since ozone is formed from oxygen atoms and oxygen molecules

$$O + O_2 \rightarrow O_3. \tag{5.5}$$

Two possible O-atom formation routes are through the hydrogenation of HO_2

$$H + HO_2 \rightarrow H_2O + O, \tag{5.2c}$$

and the reaction OH with molecular oxygen

$$OH + O_2 \rightarrow HO_2 + O. \tag{5.6}$$

Both reactions are discussed in more detail in § 5.4.1.

Sivaraman et al. (2007) also observed a temperature dependence for O_3 production after electron bombardment of an O_2 ice. They attributed this to O atoms which are more likely to react together to form O_2 than to form O_3 with O_2, even in an O_2 dominated environment. The amount of formed O_3 decreases with temperature in oxygen-rich environments for this reason. At higher temperatures, O atoms become mobile and are more likely to find reactive species like O atoms before reacting with O_2. Similar processes may be at play here and give a similar temperature dependence at low H/O_2 ratios.

For high H/O_2 ratios, reaction (5.5) competes with

$$O + H \rightarrow OH, \tag{5.7}$$

which should proceed without any barrier. We expect that the relative contribution of reaction (5.5) increases with temperature since the lifetime of H atoms on the surface, responsible for the competing reaction, decreases. A second possible mechanism that could be responsible for the detection of ozone at high temperatures is the increased penetration of hydrogen atoms into the O_2 ice with temperature as discussed in Chapter 4. Oxygen atoms are formed through hydrogenation reactions as is addressed in more detail in § 5.4 of the present chapter. At high temperatures H atoms can penetrate deeper into the ice and

therefore oxygen atoms form deeper in the ice, which in turn lead to deeply embedded ozone molecules. The chance of hydrogenating species that are positioned deep in the ice is lower than for surface species, even at high temperatures, since newly formed products at the surface and the constant deposition of O_2 can block further penetration. The ozone molecules therefore remain embedded in the ice, whereas at lower temperatures they can react further. Ozone can react with hydrogen atoms to form OH and O_2

$$O_3 + H \rightarrow OH + O_2 \tag{5.8}$$

which both can react further to water. The hydrogenation scheme of pure ozone ice is the topic of a separate paper and confirms water formation upon hydrogenation of a pure O_3 ice (Chapter 6). We expect that the detection of ozone for high H/O_2 ratios and high temperatures is due to a combination of a more effective formation and a less effective destruction at high temperatures.

Ozone is also detected in Chapter 4 upon hydrogenation of a pre-deposited pure O_2 ice and its abundance is observed to increase with ice temperature. The experimental conditions in Chapter 4's experiments can be best compared to the high H/O_2 conditions of the present chapter. We therefore expect that the effect of penetration at high temperatures is the dominant mechanism responsible for the ozone formation.

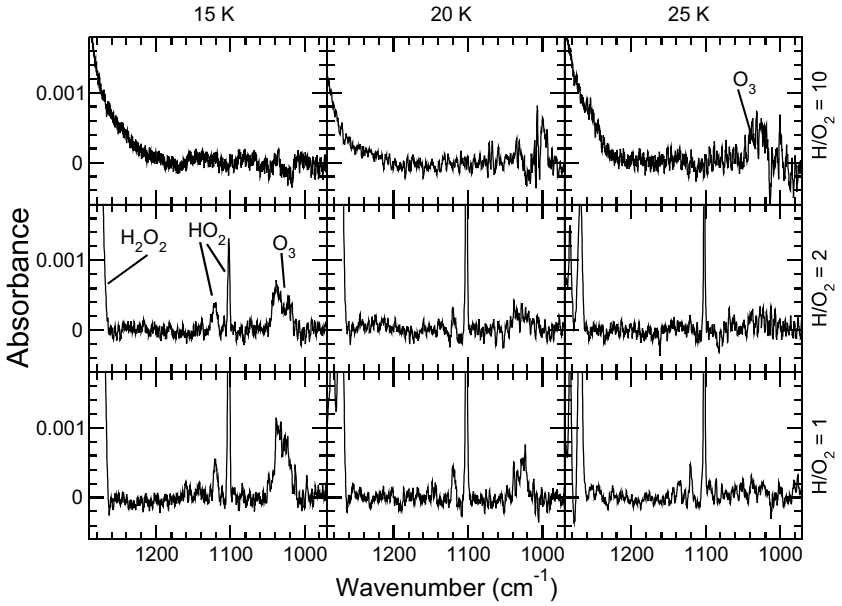

Figure 5.3 RAIR spectra of H and O_2 co-deposition experiments performed for three different surface temperature (15, 20, and 25 K) and three different H/O_2 ratios (10, 2, and 1). The spectra are zoomed in on the 1038 cm^{-1} ozone region.

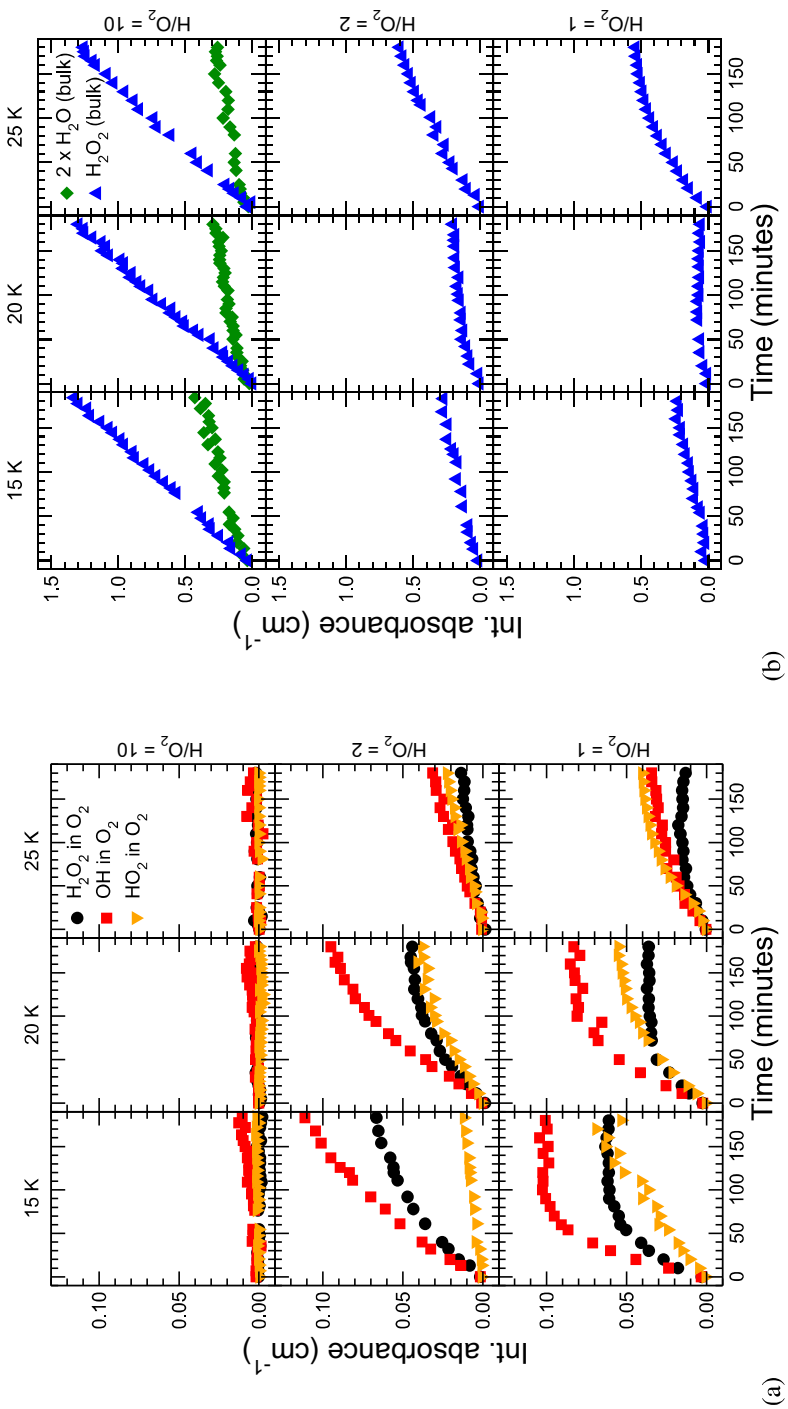

Figure 5.4 The integrated absorbance for (a) H_2O_2 in an O_2-rich environment (*circles*), OH (*squares*), and HO_2 (*triangles*) and for (b) the 1370 cm^{-1} H_2O_2 bulk and the 1650 cm^{-1} H_2O bulk features as a function of time for three different surface temperatures and three different H/O_2 ratios. The H_2O bulk integrated absorbance (panel (b)) is multiplied by a factor of two.

5.3.3 Time/fluence dependence

The production of H_2O_2, OH, HO_2 and H_2O is followed by integration of their time resolved infrared features. Figure 5.4a plots the time evolution for the integrated absorbance of the monomer features of H_2O_2, OH, and HO_2 in O_2 at different temperatures (15, 20, and 25 K) and H/O_2 ratios (H/O_2 = 10, 2, and 1). Figure 5.4b shows the corresponding evolution of the H_2O_2 and H_2O bulk features. Note that the latter signals are stronger. As mentioned before, the H_2O features in O_2 are not observed and the bulk water abundance is only shown for H/O_2 = 10, since for the low ratios, the observed water bending features are not distinguishable from the background contributions.

The H_2O_2 monomer features (black diamonds in Fig. 5.4a) follow the same trends and curve shapes as the OH abundance (squares in Fig. 5.4a). Also the H_2O and H_2O_2 bulk features (Fig. 5.4b) seem to follow each other, although not as tightly. The HO_2 abundance has its own distinct behavior. The three different trends are discussed separately below, starting with HO_2. The integrated intensities are plotted as a function of time and not of fluence, since two different species (H and O_2) are simultaneously deposited during these experiments. After 180 minutes an H-atom fluence of 3×10^{17} atoms cm^{-2} is reached; the total O_2 fluence depends on the H/O_2 ratio.

HO_2 monomer features.

The HO_2 abundance is only detectable for low H/O_2 ratios and appears to exhibit only a small temperature dependence, with 20 K as a rough estimate for the optimum temperature. The total production rate of species in general consists of different components and depends on the balance between several formation and destruction reactions. The overall rate of each individual reaction (production rate) is determined by the rate at which the reactants meet (meeting rate) and by the probability that these species react upon meeting each other (reaction rate). The first depends on the diffusion and desorption rates of the reactants; the second on the existence of a reaction barrier and the likelihood to cross this barrier if necessary. The meeting rate first increases with temperature since the species will become more mobile, but once the desorption temperature of (one of) the reactants is reached, it decreases again. The reaction rate is probably independent of temperature when no barrier exists or when the reaction proceeds through tunnelling; in the case of a thermally activated reaction, the reaction rate will increase with temperature. In the present chapter, we will try to disentangle both contributions (meeting vs. reaction rate). For the purpose of astrochemical models, the reaction rates are used as direct input parameters.

Let us consider to the production rate of HO_2. Since the production of H_2O_2 and OH (monomers) is higher at lower temperatures, the reason for the reduced HO_2 abundance at lower temperature lies probably in the more efficient destruction and not in the reduced formation of HO_2. At 25 K, the lifetime of H atoms on the surface is significantly shorter than at 20 K and this is probably the rate limiting factor for HO_2 production at higher temperatures. These arguments suggest that the HO_2 formation rate is actually temperature independent, *i.e.*, the observed temperature dependence of the production rates is

because of a temperature-dependent meeting rate. This is in agreement with gas phase calculations of reaction (5.1), where for certain incoming angles no barrier was observed (Sellevag et al. 2008, Troe & Ushakov 2008).

During the co-deposition experiment an ice builds up slowly and surface reactions will predominantly occur in the top layers, determined by the temperature dependent penetration depth as discussed in Chapter 4. If the lower layers of the ice are completely inert, one would expect the absorbance for all species to grow linearly with time. The HO_2 absorbance clearly levels off at later times (Fig. 5.4a), which suggests that some HO_2 is destroyed in the ice. Cooper et al. (2008) suggested a destruction channel via

$$HO_2 + HO_2 \rightarrow H_2O_2 + O_2 \tag{5.9}$$

in H_2O+O_2 UV irradiated ices. The HO_2 radicals, in that study and here, are formed through reaction (5.1). The hydrogen atoms originate from different sources (H-atom beam vs. photolysis). Cooper et al. (2008) found reaction (5.9) to be dominant in the case that HO_2 was formed in confined O_2 clusters where they were in close vicinity of other HO_2 radicals and the radicals did not have to travel over large distances in order to meet. In our O_2 dominated ices, HO_2 radicals are probably formed homogeneously across the ice and the HO_2 will therefore be, for similar densities, at larger average distances from each other and need to diffuse through the ice before they can react together. We do not see evidence for an increase in the destruction of HO_2 with temperature which would correspond to a thermally activated process such as diffusion. Furthermore, the products of reaction (5.9), H_2O_2 and O_2, would result in an increase of the H_2O_2 monomer features at the same time that the HO_2 disappears. However, these features appear to decrease instead of increase. We therefore conclude that HO_2 most likely falls apart in H atoms and oxygen molecules.

In Chapter 4, HO_2 is observed at the end of hydrogenation experiments at high temperatures ($T > 25$ K). We expect that HO_2 under these circumstances is formed deep in the ice and that the destruction of HO_2 by reaction with H atoms is limited in the same way as the destruction of ozone, as explained earlier.

H_2O_2 and OH monomer features.

The H_2O_2 monomer features and the OH abundance follow the same trends and are discussed together. These features are more temperature and H/O_2 ratio dependent than the HO_2 features. For H/O_2 = 1, they initially increase, then decrease and reach a steady state for the investigated temperatures, whereas for H/O_2 = 2, they only increase, although not linearly. Since both features follow each other rather tightly, OH and H_2O_2 are probably formed and destroyed by related processes. This implies that OH is formed earlier in the reaction scheme than through reaction (5.3). We will come back to this later. The decrease of both the OH and H_2O_2 signals (Fig. 5.4a) appears to coincide with the growth of the H_2O_2 bulk and H_2O contributions (Fig. 5.4b). This is a sign typical for segregation and is caused by diffusion of H_2O_2, by O_2 leaving the H_2O_2 matrix ,or a combination of both. Since the interaction between H_2O_2 and the O_2 matrix is rather weak, H_2O_2 may have a

higher mobility than usually observed in a hydrophilic environment. The mobility of O_2 is probably also rather high, since the temperature is close to the desorption temperature of O_2. This makes segregation through O_2 diffusion the most plausible scenario (Acharyya et al. 2007). In a similar fashion mobile OH can react with another OH or H_2O_2 to form H_2O_2 or H_2O, respectively, through

$$OH + OH \rightarrow H_2O_2 \tag{5.10}$$

and

$$OH + H_2O_2 \rightarrow H_2O + HO_2. \tag{5.11}$$

The first reaction is probably rather inefficient judging from the amount of OH that is present in the co-deposited ices. The hydroxyl radicals are formed in each others vicinity, since they are formed in pairs in the same reaction (see reaction (5.2b) in the next section) and the reaction of the two OH radicals is therefore not diffusion limited, but limited by the reaction probability which does not have a 100% efficiency. Another possibility for mobile OH would be to cluster inside the H_2O_2 bulk aggregates. This will probably lead to a shift and broadening of the OH features causing them to overlap with the broad 3300 cm^{-1} band. The disappearance of the 3426 and 3463 cm^{-1} OH features therefore not necessarily means that OH itself disappears but it may be due to an overlap with the polar bulk features when OH itself is in a more polar environment. Probably a critical amount of OH and H_2O_2 needs to be present before segregation occurs (Öberg et al. 2009a). This would explain why the disappearance of the OH and H_2O_2 monomer features becomes more effective at later times. As mentioned in Cooper et al. (2008), Öberg et al. (2009c) the mobility of OH is thermally activated and only becomes accessible in a water matrix above 80 K. In an oxygen matrix, which is less rigid, this could proceed at lower temperatures. The present data indicates this to be around 25 K. The strong decrease in OH and H_2O_2 monomers and the increase in H_2O_2 bulk and water at 25 K reflects indeed increased mobility of OH and H_2O_2.

Summarizing § 5.3.3, HO_2 forms in a barrierless reaction from H and O_2 and it either reacts further to OH and H_2O_2 or it slowly falls apart in H and O_2. Bulk H_2O and H_2O_2 are mostly formed for a high H/O_2 ratio and they appear to form mostly at later times, which is consistent with their formation in a late stage of the reaction scheme.

5.4 Implications for the reaction network

In this section a consistent reaction scheme is derived that explains the experimental observations described in the previous sections. This scheme is schematically presented in Fig. 5.5. This figure indicates the three initially proposed hydrogenation channels: O, O_2, and O_3 hydrogenation by the black arrows. These three channels run vertically in three columns and have the last step in common: reaction (5.4) or

$$H_2 + OH \rightarrow H_2O + H \tag{5.12}$$

to form H_2O from OH. In this section we add the reactions indicated by the light gray and dark gray arrows to this scheme. The arrow type (*solid, dashed or dotted*) reflects

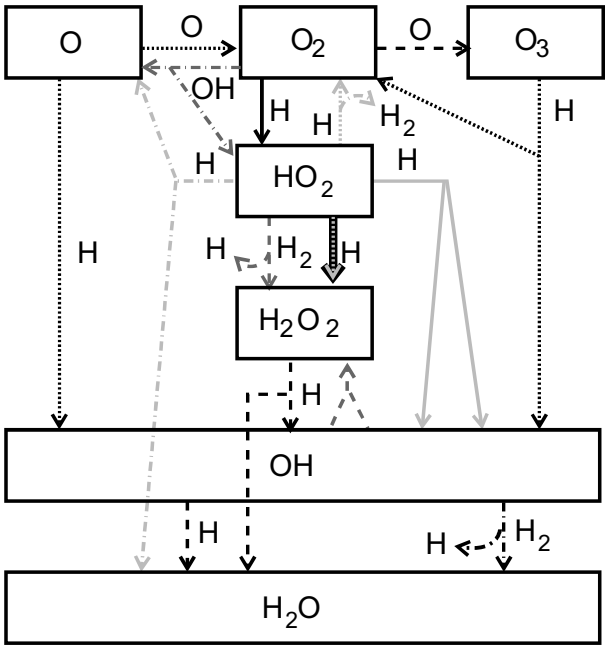

Figure 5.5 A schematic representation of the reaction network as obtained from the present study. Four types of reactions are distinguished: efficient, effectively barrierless, reactions (*solid*), reactions with a barrier but with detectable efficiency (*dashed*), reactions of which the efficiency is below the detection limit (*dash-dotted*), and reactions of which the efficiency could not be determined in this study (*dotted*). The light gray arrows indicate the same entering channel but with different outgoing channels, and the black arrows the reactions which were in the original reaction scheme.

the efficiency of the reaction. The solid arrows in Fig. 5.5 indicate the reactions that are effectively barrierless at low temperatures, the dashed lines proceed with a barrier but have a detectable efficiency, the dash-dotted arrows correspond to reactions that proceed below the detection limit, and the dotted arrows indicate reactions which were observed to proceed, but of which the efficiency could not be determined in this study. In the remainder of this section we will discuss each reaction indicated in Fig. 5.5 separately.

5.4.1 Co-deposition experiments

We first focus on the formation of OH. In the original reaction scheme (black arrows in Fig. 5.5), OH is only formed in the last reaction step. However, as mentioned before, the fact that OH is observed for low H/O_2 ratios and follows the H_2O_2 behavior suggests a common formation route. Indeed in the gas phase, the reaction of atomic hydrogen with

HO_2 is known not only to lead to H_2O_2 through reaction (5.2a)

$$H + HO_2 \rightarrow H_2O_2, \tag{5.2a}$$

but also to result in:

$$H + HO_2 \rightarrow 2OH, \tag{5.2b}$$

$$H + HO_2 \rightarrow H_2O + O, \tag{5.2c}$$

and

$$H + HO_2 \rightarrow H_2 + O_2. \tag{5.2d}$$

In the gas phase branching ratios of 0.90±0.04, 0.08±0.04, and 0.02±0.02 are found for channels (5.2b)-(5.2d), respectively (Keyser 1986). Channel (5.2a) is very unlikely in the gas phase without the presence of a third body. This channel is however allowed in the solid phase. If all four reaction channels would proceed, OH could be formed directly through channel (5.2b) or indirectly through channel (5.2c) after O has reacted to OH or to O_3 which can further react to OH.

In all experiments with $H/O_2 \leq 2$, the ratio between the produced OH and H_2O_2 abundance is constant. This already suggests that OH is mainly formed directly through channel (5.2b), since OH production through subsequent hydrogenation after channel (5.2c) would lead to an OH production as function of time differently from the H_2O_2 production.

Assuming that all detected OH is indeed formed through channel (5.2b), the branching ratios between the OH and H_2O_2 formation channels in the solid phase can be obtained. The 2OH channel (5.2b) is found to be 1.6±0.2 times more likely than the H_2O_2 channel (5.2a), provided that the OH-stretch bandstrength per molecule of H_2O_2 is twice as large as that of an OH radical. Another possibility could be that H_2O_2 is not formed directly through reaction (5.2a) but that in (38±5)% of the cases two OH molecules immediately react and form H_2O_2 (reaction (5.10)). Since OH is still abundantly observed and since most OH is formed through reaction (5.2b) which results in two OH radicals in close vicinity of each other, this reaction will proceed with some barrier. It is therefore indicated by a dashed light gray arrow in Fig. 5.5; the double arrow coming from OH reflects the two OH molecules that are needed in the reaction.

Unfortunately, we cannot quantify channel (5.2d) (H_2+O_2) since both products are not infrared detectable and the change in the water-induced O_2 feature at 1550 cm^{-1} caused by this reaction will be too small to derive a reliable branching ratio.

The branching ratio of the channel leading to H_2O and O (channel (5.2c)) is also hard to quantify, since O atoms can only be detected indirectly by the production of ozone. In the low H/O_2 regime, the OH-stretch modes which are used to quantify the branching ratios for the 2OH and H_2O_2 channels cannot be used for H_2O, since the OH-stretch modes for water in O_2 are below the detection limit. However, using this detection limit, the reactive rate for channel (5.2c) can be constrained to an upper limit of 0.2 times the value of the H_2O_2 channel. This upper limit is 0.08 with respect to combined rate of channels (5.2a) and (5.2b), close to the gas phase branching ratio. The low upper limit further justifies our assumption that OH is mostly formed through channel (5.2b), since

only a limited amount of atomic oxygen, needed for the O and O_3 routes, is formed through channel (5.2c).

The light gray arrows in Fig. 5.5 indicate the four different channels for the H + HO_2 reaction. In § 5.3.3 we have argued that reaction (5.1) is barrierless. This reaction is therefore represented by solid arrows. Since in Chapter 4, HO_2 is not observed for $T < 25$ K, the reaction of H + HO_2 is probably effectively barrierless as well, which is in agreement with gas phase data where no barrier is observed between 245−300 K (Keyser 1986). The main channel, (5.2b), is therefore also represented by solid light gray arrows. Channels (5.2a) and (5.2d) cannot be measured directly as discussed above and are therefore represented by dotted arrows. For channel (5.2c) only an upper limit is determined and is therefore represented by a dash-dotted light gray arrow.

Ozone is formed through reaction (5.5) and proceeds with a barrier as discussed earlier. This reaction is therefore indicated by a dashed black arrow in Fig. 5.5. The fact that O_3 is observed, means that O atoms are involved in the reaction network. One O-atom formation route is through reaction (5.2c). The reaction

$$OH + O_2 \rightarrow HO_2 + O, \tag{5.6}$$

which has a gas phase barrier of 220 kJ/mol (Tsang & Hampson 1986), is another likely candidate, if it could proceed through tunnelling which has little temperature dependence. As discussed earlier, the OH features are observed to disappear mostly through a thermally activated diffusion process and reaction (5.6) is therefore thought not to have a large effect on the total OH abundance. In conclusion, the O atoms are probably formed through two relatively inefficient reactions: reactions (5.2c) and (5.6). The observed OH is therefore mainly formed by reaction (5.2b). Since reaction (5.6) is uncertain it is indicated by dash-dotted dark gray arrows in Fig. 5.5.

5.4.2 Hydrogenation of H_2O_2

Water is likely to be formed through a number of different reaction paths in the network: by the hydrogenation of HO_2, OH or H_2O_2. The first, reaction (5.2c), is relatively inefficient as discussed in § 5.4.1. Leaving the other two as as the dominant routes. In this subsection we discuss the specific contribution of H_2O_2 hydrogenation to the overall H_2O production. This route proceeds via reactions (5.3) and (5.4). The first has a barrier in the gas phase of 14.97 kJ/mol (Baulch et al. 1992) and consequently a lower efficiency is expected for H_2O formation through this reaction. The most straightforward way of testing this reaction would be to deposit a pure H_2O_2 ice and subsequently expose this to H atoms. However, since the deposition of H_2O_2 without simultaneous H_2O deposition is not experimentally feasible in our set-up, pure H_2O_2 ice is produced in a different way. At the end of a co-deposition experiment with an H/O_2 ratio of 10, the ice is dominated by H_2O_2 and O_2 (see Fig. 5.2). By heating the ice to 40 K, all the O_2 desorbs from the top, reactive layers, and the resulting bulk H_2O_2 ice can be used for a hydrogenation experiment in which the last part of the reaction scheme (reactions (5.3) and (5.4)) can be studied. In this specific case the ice is exposed to H atoms after it is formed, as in Chapter 4 (in

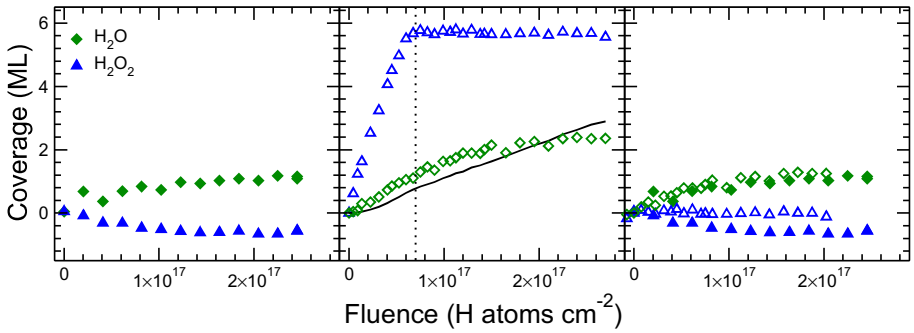

Figure 5.6 The H_2O and H_2O_2 surface coverage in monolayers at 20 K for a H_2O_2 hydrogenation experiment (*filled symbols*) and O_2 hydrogenation experiment (*open symbols*). The right panel compares the H_2O_2 and the O_2 hydrogenation experiment after a fluence of 7×10^{16} atoms cm^{-2} (*dotted line in middle panel*). The solid curve in the middle panel indicates the calculated contribution of water formation from reaction (5.3) (Eq. 5.13).

contrast to the experiments discussed in the rest of the present chapter where H atoms and O_2 molecules are co-deposited). The left panel of Fig. 5.6 plots the H_2O and H_2O_2 surface coverage with respect to the initial H_2O_2 ice for a temperature of 20 K. Hydrogen peroxide is used up whereas H_2O is formed. To obtain the absolute quantities from the integrated absorbances, the apparent bandstrength for water (0.02 cm^{-1}ML^{-1}) as determined in Chapter 4 is used. The corresponding value for H_2O_2 is obtained from this experiment by assuming mass balance. A H_2O(1580−1800 cm^{-1})/H_2O_2(1200−1580 cm^{-1}) ratio of 0.31 is obtained in accordance with Loeffler et al. (2006).

This experiment can be directly compared to the hydrogenation experiments of solid O_2 as reported in Chapter 4. Both the deposition technique (sequential deposition of the ice and H atoms instead of simultaneous) and the experimental conditions in terms of surface temperature and H-atom flux are the same. The middle panel plots the H_2O and H_2O_2 surface coverage as a function of time for an O_2 hydrogenation experiment, again at 20 K. The efficiency of the destruction reaction (5.3) can be determined by comparison of the combined formation reactions (5.1) and (5.2a). In the middle panel (5.3±0.7)×10^{-17} monolayers of H_2O_2 are formed per deposited H atom per cm^2 (slope of the first part of the curves with triangles). It takes two H atoms to form one H_2O_2 molecule. In the left panel (2.8±0.7)×10^{-18} monolayers of H_2O_2 are destroyed per deposited H atom per cm^2 (slope at zero fluence of the curves with triangles). It takes also two H atoms to destroy one H_2O_2 molecule. The H_2O_2 destruction reaction (reaction (5.3)) is the rate limiting step in the formation of water — reaction (5.4) is more efficient. The rate of reaction (5.3) can therefore be quantified with respect to the rate of reaction (5.2a), $k_{5.2a}$, which is (2.8±0.7)×10^{-18}/(5.3±0.7)×10^{-17} = (0.05±0.01)$k_{5.2a}$. This lower efficiency with respect to $k_{5.2a}$ indicates that there is a barrier for reaction (5.3) and it is therefore indicated by a dashed black arrow in Fig. 5.5.

The water formed in the O_2 hydrogenation reactions (*middle panel*) can be formed

through several reaction routes. The most important two are reactions (5.3) and (5.4). The solid line in the middle panel of Fig. 5.6 shows the contribution of reaction (5.3). This line is obtained from

$$N_{\text{reaction (5.3)}}(H_2O) = 2 \cdot 2.8 \times 10^{-18} F \frac{N(H_2O_2)}{N_{\max}(H_2O_2)} \tag{5.13}$$

with F the hydrogen fluence in atoms cm^{-2}. The factor of 2 accounts for the stoichiometric ratio in O atoms between H_2O and H_2O_2, the rate of 2.8×10^{-18} ML cm^{-2} is taken from the H_2O_2 hydrogenation experiment and the last term in this expression accounts for the probability of an H atom to meet H_2O_2 where the maximum amount of formed H_2O_2 corresponds to the starting condition of the H_2O_2 hydrogenation experiment. Reaction (5.3) accounts for (30±5)% of the formed H_2O in the beginning of the O_2 hydrogenation experiment by comparing the slope of the solid line and the slope of the experimental water abundance (*open diamonds*) at the beginning of the experiment. After 7×10^{16} atoms cm^{-2}, when the maximum amount of H_2O_2 is reached (*vertical dotted line*), the route accounts for roughly 70% of the formed water as is shown in both the middle and the right panel of Fig. 5.6. In the right panel the results of the H_2O_2 hydrogenation experiment are overplotted by the O_2 hydrogenation results after 7×10^{16} atoms cm^{-2}. The H_2O_2 production has reached its maximum at that fluence and the resulting ice is probably similar to the initial condition of the H_2O_2 hydrogenation experiment. The hydrogen peroxide use-up in the O_2 hydrogenation experiment is roughly half of the case where H_2O_2 is hydrogenated (comparison open and closed triangles in right panel) while an equal amount of water is formed (comparison open and closed diamonds in right panel). Part of this is within the error.

Let us now return to the beginning of the O_2 hydrogenation experiment when (30±5)% of the formed H_2O is formed via reaction (5.3). The remaining (70±5)% is most likely formed through reaction (5.4) as discussed earlier. From the co-deposition experiments we know that the reaction of H and HO_2 leads to 3.2 times more OH than H_2O_2, however, only a small amount of water is formed from all these hydroxyl radicals. If OH does not react to H_2O_2, $3.2 \times 5.8 = 19$ ML OH should have formed during the first part of the O_2 hydrogenation experiment. Only $0.70 \times 1.2 = 0.8$ ML of water has been formed from these OH radicals, which amounts to (4±1)%. Since reaction (5.4) is barrierless, this low efficiency is rather surprising. A reason for this could be that the majority of the OH radicals reacts together in the bulk of the ice and would be responsible for part of the H_2O_2 contribution. However, as discussed earlier, we would not expect this to happen in large quantities based on the co-deposition experiments. Another possibility could be that H atoms are not able to reach all OH radicals in the ice. An argument against this is that O_2 still reacts, which means that the ice is not impenetrable. However, it could be that only H-atom approaches under specific incoming angles to OH are reactive, whereas the number of reactive configurations for H reacting with O_2 is much larger. To reflect the relatively low efficiency of this reaction, this reaction is indicated with a dashed black arrow in Fig. 5.5.

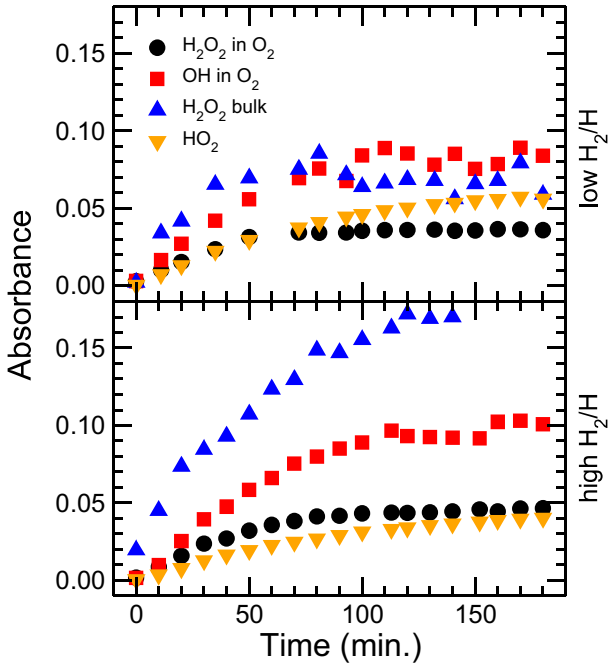

Figure 5.7 RAIRS integrated intensities for $H/O_2 = 1$ and at 20 K with two different H/H_2 ratios. The standard, low, H_2/H ratio results are plotted in the upper panel; the high H_2/H ratio results in the lower panel.

5.4.3 The role of H_2

All reactions discussed in the previous sections ignore the presence of H_2 in the atom beam. However, H_2 will also be present on the surface, mostly from direct deposition of cold molecules from the atom beam, since formed H_2 on the surface is likely to desorb upon formation. If H_2 and O_2 are co-deposited, no reactions are observed, only background deposition of H_2O. However, in the presence of H atoms new reactive species are formed that can react with H_2, in particular OH to form H_2O (reaction (5.12)) or HO_2

$$H_2 + HO_2 \rightarrow H_2O_2 + H. \tag{5.14}$$

By changing the temperature of the filament in the H-atom source and the H_2 pressure in the atomic line, we can keep the H-atom flux constant while increasing the H_2 flux. Figure 5.7 plots the resulting integrated intensities for such an experiment in the lower part. Here the H_2 flux is roughly ten times higher than in the regular experiments ($H/H_2 = 90$ vs. $H/H_2 = 9$ in the standard experiments). The difference in H_2 abundance is therefore definitely due to a change in the cold molecule abundance, since the contribution of formed H_2 molecules remains the same. If reaction (5.12) were efficient, the OH

radicals that are formed would react further to H_2O in the high H_2/H experiment and we would be able to observe a significant decrease in the OH surface abundance in the bottom panel with respect to the top panel. At the same time we would expect to be able to detect H_2O in the high H_2/H spectra. Figure 5.7 does however not show such a decrease in OH abundance and also H_2O monomer features were not detected in the IR spectra. We therefore conclude that reaction (5.12) is not very efficient (dash-dotted black arrow in Fig. 5.5). Gas phase experiments show a barrier of 12.69 kJ/mol in the low temperature limit (Orkin et al. 2006).

In the surface abundances of HO_2 and H_2O_2 on the other hand a change can be observed. The abundance of HO_2 decreases in the high H_2/H regime whereas H_2O_2 increases. This is in accordance with reaction (5.14) and this reaction is therefore indicated by a dashed dark gray arrow in Fig. 5.5. The fact that reaction (5.14) proceeds at such low temperatures, is rather surprising since a high gas phase barrier of 109 kJ/mol was reported for this reaction (Tsang & Hampson 1986). An explanation for this is not available.

5.5 Conclusions

The present study shows that the water formation reaction network as originally proposed by Tielens & Hagen (1982) is not complete but that several new reaction paths should be added. The solid state hydrogenation of O_2 exhibits a complex network of reactions as schematically presented in Fig. 5.5. The original reactions are indicated in black. The dark gray and light gray reactions are added in the present study. Through this effort we have shown that the O_2 hydrogenation channel is connected to the O and O_3 hydrogenation channels and we have therefore been able to also draw conclusions on some reactions which are part of the other two hydrogenation channels. We could furthermore quantify the reaction rates of several reactions.

The solid arrows in Fig. 5.5 indicate the reactions that are effectively barrierless at low temperatures. These consist of two reactions

$$\mathrm{H + O_2 \rightarrow HO_2}, \tag{5.1}$$

and the reaction of HO_2 and H atoms, indicated in dark gray. The latter has probably four different product channels:

$$\mathrm{H + HO_2} \rightarrow \begin{cases} \mathrm{H_2O_2} & k_{5.2a}, \\ \mathrm{2OH} & (1.6 \pm 0.2)k_{5.2a}, \\ \mathrm{H_2O + O} & (< 0.2)k_{5.2a}, \\ \mathrm{H_2 + O_2} & \end{cases} \tag{5.2}$$

where the last product channel cannot be quantified by the methods used in this experimental study.

The reactions which are indicated by the dashed lines proceed with a barrier but have a detectable efficiency. These reactions include:

$$\mathrm{H + H_2O_2 \rightarrow H_2O + OH} \qquad (0.05 \pm 0.01)k_{5.2a}, \tag{5.3}$$

$$H + OH \rightarrow H_2O, \tag{5.4}$$

$$H_2 + HO_2 \rightarrow H_2O_2 + H, \tag{5.14}$$

and

$$2OH \rightarrow H_2O_2. \tag{5.10}$$

The dash-dotted arrows indicate reactions that have been proposed but which are not observed to proceed in this study, either because the reaction is too slow or because the experimental method did not allow us to detect this reaction. The reactions

$$H_2 + OH \rightarrow H_2O + H, \tag{5.12}$$

$$H + HO_2 \rightarrow H_2O + O \qquad (< 0.2)k_{5.2a}, \tag{5.2c}$$

and

$$OH + O_2 \rightarrow HO_2 + O \tag{5.6}$$

were found to proceed with efficiencies below our detection limit. The reaction

$$H + HO_2 \rightarrow H_2 + O_2 \tag{5.2d}$$

cannot be detected by the methods used in this experimental study. The same is true for the direct channel of

$$H + HO_2 \rightarrow H_2O_2 \tag{5.2a}$$

which could proceed with 2OH as intermediates.

The dotted arrows indicate reactions that were found to proceed, but of which the efficiency could not be determined in this study. The reaction

$$H + O \rightarrow OH \tag{5.7}$$

is most likely barrierless. From the the present study we can conclude that it is more efficient than the formation of ozone from oxygen atoms. Since the amount of formed ozone cannot be quantified, the efficiency of the reaction

$$H + O_3 \rightarrow O_2 + OH \tag{5.8}$$

could not be determined from this study. Studies of the hydrogenation of ozone indicate this reaction to be efficient.

This studies shows that in the O_2 hydrogenation experiments performed in Chapter 3 and 4, and Miyauchi et al. (2008) water is formed through different reaction paths. Especially in the early stage of experiment, H_2O is not predominantly formed through the hydrogenation of H_2O_2 but through the reaction with OH. By not considering the latter route in the model to fit to the experimental data, an artificial, isotope-independent reaction rate has been obtained for the $H + H_2O_2$ reaction as explained in the introduction.

This newly determined reaction scheme will have profound implications for models that model the formation of water under interstellar conditions. Clearly several new reaction paths should be considered through this study. Moreover, several reactions proved to be much more efficient ($H + O_2$) or less efficient ($O + OH$ and $H_2 + OH$) than originally thought. A dedicated study in which this new scheme will be the input of a new model needs to be applied to tell us how this will affect the formation of interstellar water under different interstellar conditions exactly.